A 50 Gb/s Transparent Indoor Optical Wireless Communications Link with an Integrated Localization and Tracking System

Ariel Gomez, Kai Shi, Crisanto Quintana, Grahame Faulkner, Benn C. Thomsen, *Member IEEE* and Dominic O'Brien, *Member IEEE*

***Abstract*—In this paper we describe an optical wireless communications system that uses light from an optical fibre access point to provide transparent and bi-directional optical links to nomadic terminals. Full localization and tracking is implemented, and a 50Gb/s link is demonstrated. The link operates in an indoor environment, with a ±30° field-of-view covering a distance of up to 3 m, and a localization accuracy of 0.05° (2.5 mm pointing accuracy at 3 m) is achieved. This demonstration shows it is feasible to use an automated system to achieve the required alignment for an ultra-high data rate fibre-wireless-fibre link.**

***Index Terms*— Optical wireless communication, beam steering, infrared tracking, laser beam steering, spatial light modulator.**

I. Introduction

TRAFFIC from wireless and mobile devices is predicted to increase 10-fold between 2014 and 2019, surpassing wired data traffic by 2016 [1]. Given the expected RF capacity crunch [2], this growing demand will have to be met using a variety of new wireless technologies exploiting other parts of the electromagnetic spectrum. Millimetre wave, Terahertz as well as Optical Wireless Communications (OWC) are all being investigated as possible approaches [3]–[8]. We focus here on ultrafast indoor OWC.

Passive optical networks PONs are being widely deployed at customer premises [9], allowing for data rates of potentially hundreds of Gb/s to reach indoor environments. This capacity can be transparently distributed to wireless devices using Infrared (IR) OWC. In our approach, a static base station (BS) connected to the fibre network, is fixed to the ceiling of a room. Light directly from the fibre forms narrow beams which are steered to nomadic terminals (NT) located throughout the coverage area. This concept was recently demonstrated for a single mode fibre (SMF)-wireless-SMF link working at a data rate above 100 Gb/s with a wide field-of-view (FOV) of ±30° [10]. The experiment was carried out with manual control of the holographic beamsteering system. In this paper, the design and implementation of a suitable localization and tracking system is described, and the operational characteristics of the automated link alignment. Although indoor localization systems have been proposed [11]–[14], to the best of our knowledge this is the first experimental demonstration of a localization and tracking system applied to ultrafast narrow beam OWC.

The paper is organized as follows: section II gives the system design of the BS and NT with the integrated localization and tracking system; section III shows the experimental results for a CW analysis as well as a coherent transmission experiment; and finally, section IV gives the conclusion.

II. System Design

The system architecture is shown in Figure 1. A fibre-fed BS is fixed to a ceiling located at ~3 metres above the room's floor. Light exiting the fibre is collimated to form a narrow 1550 nm beam. This is then steered to NTs distributed within a BS FOV of ±30°. The steering range is achieved via a combination of accurate active beamsteering using spatial light modulators (SLM) and passive angle magnification (AM) [10]. After the BS, beams propagate in free space to be collected by the NT's apertures. Inside the NT, the light is steered back into a receiver fibre using a similar AM-SLM module, to successfully establish the communications link.

For the system to operate the BS has to know the location of the NTs (and vice versa). The link is implemented using narrow optical beams, so acquisition and tracking using only these signals would be lengthy and impractical. For this reason, a separate beacon based tracking system is added. This system uses a wide FOV CMOS camera at the BS to detect the emission from near-IR LED tags placed around the NT apertures (see Figure 1). The downlink beam is then steered using the BS SLM such that the beam enters the NT. Within the NT a beamsplitter (BSp) takes a fraction of the downlink signal light (at 1550nm) to a position sensing detector (PSD). A closed-loop algorithm then uses the reading from the PSD and the NT beamsteering capability to align the beam to the

Ariel Gomez, Crisanto Quintana, Grahame Faulkner, and Dominic O'Brien are with the Department of Engineering Science, University of Oxford, Oxford OX13PJ, UK. (e-mail: ariel.gomezdiaz@eng.ox.ac.uk; crisanto.quintanasanchez@eng.ox.ac.uk; grahame.faulkner@eng.ox.ac.uk; dominic.obrien@eng.ox.ac.uk).

Kai Shi and Benn C. Thomsen are with the Department of Electronics and Electrical Engineering, University College London, London WC1E 7JE, UK. (e-mail: k.shi@ucl.ac.uk; uceesat@ucl.ac.uk; b.thomsen@ucl.ac.uk).

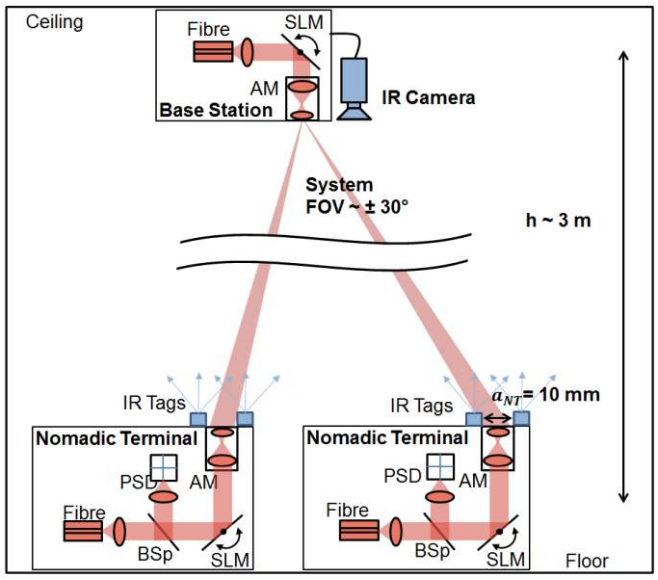

Figure 1. General architecture of a base station interacting with 2 nomadic terminals. AM is an angular magnification module, BSp is a beamsplitter and PSD is a position sensitive detector.

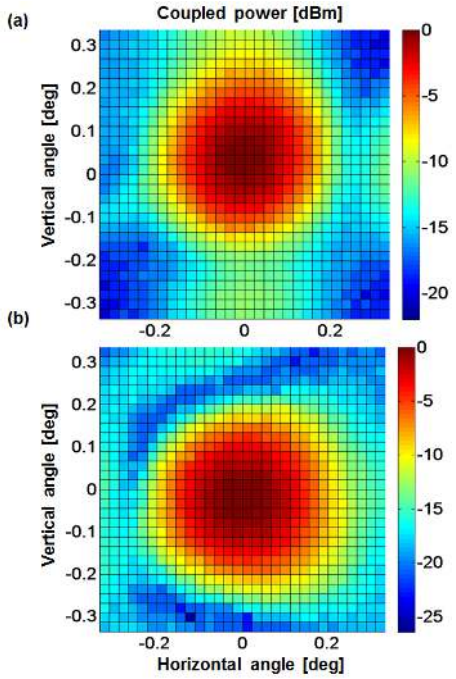

Figure 2. Experimental characterization of a SMF fibre. Normalized received power as a function of (a) BS beamsteering keeping the NT fixed and (b) NT beamsteering keeping the BS fixed. The BS and NT distance is Z~ 3 metres.

receiving fibre axis. The downlink can then be successfully established. At the same time, the uplink is automatically aligned due to the reversibility of light. This bidirectional property has been demonstrated elsewhere [10] and it holds if the wavelength of operation is close to that of the downlink [15].

In this manuscript we focus on the performance of a single downlink beam, but the use of a camera at the BS allows multiple terminals to be located and a point-to-multipoint system to be implemented. In the following sections details of the tracking system are described.

A. IR beacon localization system

The NT aperture diameter a_{NT} = 10 mm and the communications beam has a diameter of ~10 mm at a BS-NT distance of 3 m [10]. This small aperture and narrow beam combination determines the BS required steering accuracy. Figure 2 (a) shows the NT coupled power vs. the BS steering angle for an SMF-wireless-SMF link. It can be seen that a steering accuracy of 0.1º is needed to have a coupling loss under 3dB. This translates into a pointing accuracy of ~ 5 mm at a BS-NT distance of 3 m. In the next section, a beacon design to meet these requirements is described.

1) Beacon design

Near-IR beacons are placed next to the NT such that the CMOS camera locates the centre of the NT aperture. A 12-LED array was designed to circle this aperture with a diameter of $\emptyset_{LED}$ = 50 mm. Each LED (OPTEK OP291A) has an emission angle of ±50º which is sufficient for the system design FOV of ±30º. The wavelength of operation is 890 nm. Figure 3 (top right inset) shows an LED ring prototype built with these specifications. The arrangement allows the BS to estimate not only the aperture position but also the distance from the BS to the NT. In operation, and ellipsoidal image of the beacon ring is captured by the IR camera, and software (MATLAB) is used to fit an ellipse to this. The centre of the ellipse gives the location of the NT aperture and the ellipsoid major axis can be used to calculate the BS-NT distance d_{NT} as follows:

$$d_{NT} = \frac{\emptyset_{LED}}{\emptyset_{CAM}} \cdot f_{CAM} \;;\; d_{NT} \gg f_{CAM} \qquad (1)$$

Here $\emptyset_{\mathrm{CAM}}$ is the major axis of the ellipse in the camera sensor plane. A high resolution camera with a low distortion imaging lens is needed to accurately determine the ellipse dimensions in the sensor plane.

2) Imaging system design

Figure 3 shows a schematic of the BS localization system. The IR camera is required to resolve the LED ring at a

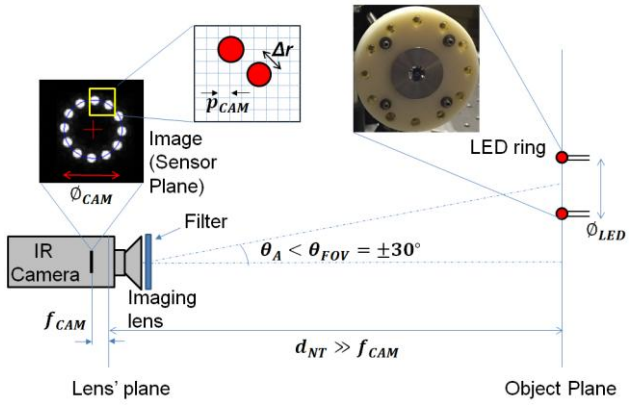

Figure 3.Schematic of the IR imaging system. The insets shows pictures of the LED ring and its image in the camera's sensor plane.

distance of up to 3 metres. Rearranging equation (1) and using diffraction arguments, the following relationships between the object and image planes are derived:

$$\emptyset_{CAM} = M_{CAM} \cdot \emptyset_{LED} = \frac{f_{CAM}}{d_{NT}} \cdot \emptyset_{LED}$$
$$\Delta r = 1.22 \cdot \frac{\lambda_{LED}}{NA} = 2.44 \cdot \lambda_{LED} \cdot F_{\#} \quad (2)$$

where M_{CAM} is the system optical magnification, λ_{LED} is the LED wavelength of operation and NA and $F_{\#}$ are the imaging lens' numerical aperture and F number, respectively. Δr is the diameter of the each individual LED image in the camera sensor plane assuming they form diffraction limited images . Evaluating equation (2) for test values d_{NT} = 3 m, f_{CAM} = 3.5 mm, $F_{\#}$ = 2.4, λ_{LED} = 890 nm and $\emptyset_{LED}$ = 50 mm, gives Δr ~ 5 µm and $\emptyset_{CAM}$ ~ 58 µm. A sensor with a pixel size $p_{CAM} < \Delta r$ = 5 µm is therefore desirable.

In addition to this, the imaging system must have a FOV > 30°. Thus, off-axis aberrations need to be minimized and a low distortion imager is required. To achieve this, an Edmund Optics CMOS camera (EO10012M) with a low distortion lens with f_{CAM} = 3.5 mm and a FOV >±40° was combined with a ½ inch sensor with p_{CAM} = 1.6 µm. A high-pass optical absorption filter was also used in front of the CMOS camera to filter the ambient light.

3) System calibration

The CMOS camera is off-axis with respect to the BS communications aperture. This implies that the localization coordinates given by the CMOS camera need to be transformed so that they are referenced to the communications beam path.

To illustrate the problem, Figure 4 shows a schematic of the BS. The camera aperture is assumed to be at the origin, with no loss of generality. The communications aperture is offset by (H_l^0, V_l^0) in the same plane. The figure also shows the output communications beam (green solid line) where $\theta_l = (\theta_l^H, \theta_l^V)$ are the link's horizontal (H) and vertical (V) angular coordinates. The intersection (H_l^1, V_l^1) and (H_l^2, V_l^2) of this beam with two arbitrary planes at distances d_1 and d_2, respectively are also given. The images of these two points in the camera sensor plane are (H_c^1, V_c^1) and (H_c^2, V_c^2), respectively, as outlined by the red dotted lines.

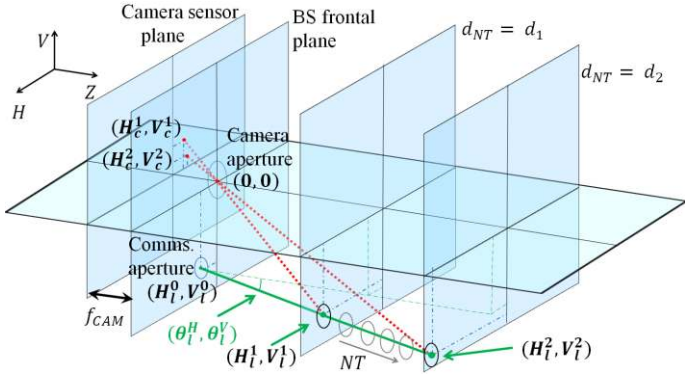

Figure 4. Schematic in 3D for a BS with off-centred communications and camera apertures. The green solid line is the communications beam. The red dotted lines are the beacon beams.

Let us assume that the beam is pointing at the NT, i.e. the NT aperture is located at (H_l^1, V_l^1) in the plane $d_{NT} = d_1$. If the NT moves to (H_l^2, V_l^2), then the communications link is still aligned but the image camera registers a shift X_{sh} given by:

$$X_{sh} = \frac{X_l^0 + d_2 \tan\theta_l^X}{1 - d_2/f_{CAM}} - \frac{X_l^0 + d_1 \tan\theta_l^X}{1 - d_1/f_{CAM}} \quad (3)$$

Where $X = \{H, V\}$ and f_{CAM} is the camera lens' focal length. Considering $d_{NT} \gg f_{CAM}$, then equation (3) simplifies to:

$$X_{sh}(d_1, d_2) = f_{CAM} \cdot X_l^0 \left(\frac{1}{d_1} - \frac{1}{d_2}\right) \quad (4)$$

Equation (4) is convenient as there is no dependence on θ_l. The system calibration consists in finding a relationship between the camera image coordinates (H_c, V_c) and the link angle $\theta_l = (\theta_l^H, \theta_l^V)$, needed to accurately point at the NT aperture with coordinates (H_l, V_l) in an arbitrary plane $d_{NT} = d$. For this purpose, a calibration plane at a distance d_{CAL} from the BS is chosen. In the camera sensor plane, the coordinates (H_c^0, V_c^0) are calculated for a test NT aperture aligned with the communications beam when no steering is applied, i.e. $\theta_l = 0$. Then, using geometric arguments it can be shown that:

$$\theta_l^X(X_c, d) = tan^{-1}\left[\frac{1}{f_{CAM}}(X_c - X_c^0 - X_{sh}(d_{CAL}, d))\right] \quad (5)$$

Equation (5) is a closed form function between the camera coordinates X_c $(X = \{H, V\})$ and the link angle θ_l using the correction $X_{sh}(d_{CAL}, d)$ as the NT range d changes. However, we have assumed an ideal steering system with linear and circular symmetry for all its components. This cannot be achieved in the experiments, particularly if a steering accuracy of 0.1° for a target FOV = ±30° is required. Therefore, further calibration is needed to find an empirical form for (5). The procedure is as follows, referring to Figure 4:

1- A calibration plane $d_{NT} = d_{CAL}$ is chosen with NT aperture coordinates (H_l^1, V_l^1).
2- A 2D scan is performed by varying (H_l^1, V_l^1) for N_{scan} points. For each scanning point, the steering action $(\theta_l^H, \theta_l^V) = h(H_l^1, V_l^1)$ and camera plane coordinates $(H_c^1, V_c^1) = g(H_l^1, V_l^1)$ are recorded. A discrete map is then established between (θ_l^H, θ_l^V) and (H_c^1, V_c^1). Functions h and g are not known in an exact form and they typically vary from setup to setup.
3- A linear interpolation is generated giving a functional fit $(\theta_l^H, \theta_l^V) = S(H_c^1, V_c^1)$. The higher N_{scan} the more accurate the fit will be.
4- For a general NT plane d, instead of equation (5), we use:

$$(\theta_l^H, \theta_l^V) = S(H_c - H_{sh}(d_{CAL}, d), V_c - V_{sh}(d_{CAL}, d)) \quad (6)$$

The procedure above is used in the experimental sections to calibrate the BS localization system.

B. NT tracking module

Once the BS points the communications beam at the NT aperture, then the NT has to steer the incoming light so it is aligned with the optical axis of the receiving fibre. Figure 1 shows a PSD based sensing system to accomplish this. A beamsplitter (BSp) is located just after the steering unit, diverting a fraction of the light to the PSD. A lens focuses this light onto the PSD plane. An iterative procedure follows, in which the SLM moves the sampled beam to the centre of the PSD. This point corresponds to the steering with optimal power coupling into the receiving fibre, provided the appropriate mechanical pre-alignment.

A proof-of-principle system based on a quadrant photodetector (Quad) was developed. In the following section the Quad-lens design is first studied. Then, we focus on the iterative algorithm to centre the beam footprint in the Quad active area.

1) Quad lens design

A schematic of the NT tracker is given in Figure 5. The communications beam reflects off an SLM with an active area of radius ω_{SLM} and a steering range $\pm\delta$. Then, it propagates for a distance d_{SLM} before illuminating a lens with aperture a_L and focal lens f_Q. This lens focuses the beam onto a Quad detector located at a distance $d_Q < f_Q$. The radius of the Quad active area is a_Q. Ray tracing theory using an ideal thin lens gives:

$$\omega_Q = \left(1 - \frac{d_Q}{f_Q}\right)\omega_{SLM}\,;\; S_L = d_{SLM}\delta\,;$$
$$S_Q = \left[\frac{\omega_Q d_{SLM}}{\omega_{SLM}} + f_Q\left(1 - \frac{\omega_Q}{\omega_{SLM}}\right)\right]\delta \qquad (7)$$

Where ω_Q is the beam footprint in the Quad plane. S_L and S_Q are the beam walk-off (see Figure 5) in the lens and quad planes, respectively. The NT tracker needs to satisfy the following conditions:

1- $S_L < a_L$ to avoid beam vignetting at the lens. An appropriate d_{SLM} based on the SLM steering range δ can be chosen.

2- $\omega_Q < a_Q$ so that the Quad active area is not overfilled. This condition can be easily achieved by tuning the lens to Quad distance d_Q in equation (7).

3- Beam walk-off $\Delta S_Q > \tau$ in the Quad plane for a beamsteering difference $\Delta\delta$. Here τ is the Quad sensitivity to beam displacements and $\Delta\delta$ is required steering accuracy.

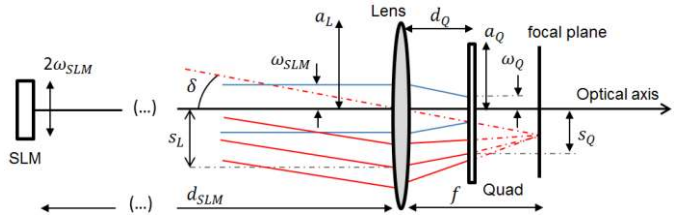

Figure 5. Quad design layout. Ray tracing from the steerer to the Quad for the un-deflected on-axis beam (blue lines) and the deflected off-axis beam (red lines).

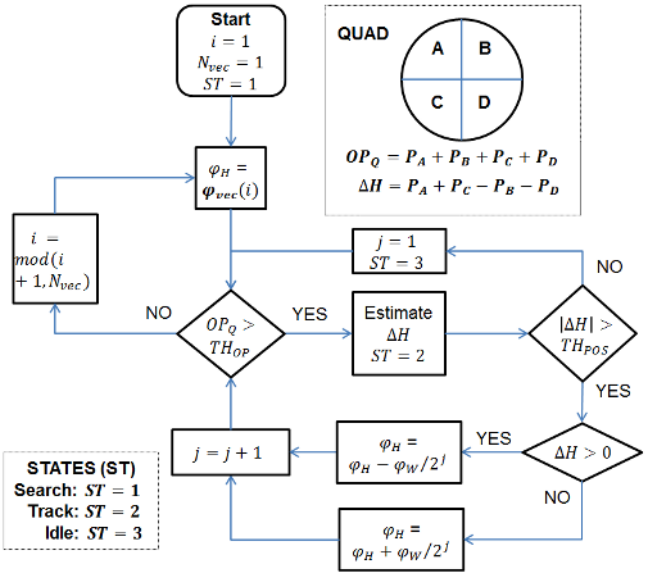

Figure 6. Flowchart for the search and iterative tracking algorithms. TH_{OP} is the optical power decision threshold in the search state. TH_{POS} is the decision threshold in the tracking state. φ_W is the constant steering increment in $\boldsymbol{\varphi_{vec}}$, i.e. $\varphi_W = \varphi_{vec}(i+1) - \varphi_{vec}(i), i = \{1,2,\dots,N_{vec}\}$.

Equation (7) shows that a lens with a large focal lens f_Q makes it easier to meet the 3rd condition by enhancing the beam walk-off on the Quad to achieve $\Delta S_Q > \tau$.

2) Quad search and tracking algorithm

The previous section described a valid Quad lens design. However, a lens with a large focal length f_Q causes a beam-walk-off range in the Quad plane, assuming $d_Q \sim f_Q$ is $S_Q(\pm\delta) = \pm\delta \cdot f_Q$. This corresponds to a full displacement window of $2\delta \cdot f_Q \gg 2a_Q$ in the Quad plane, which is $N_{vec} = \delta \cdot f_Q / a_Q$ times larger than the Quad active area diameter $2a_Q$. Therefore, a search algorithm is first needed to bring the beam spot to the Quad active area, followed by an iterative procedure to centre the spot in the Quad. The corresponding flowchart is shown in Figure 6 for a 1D horizontal axis.

In the Quad plane, the horizontal axis is divided into small windows of size $2a_Q$. The search initial state ($ST = 1$) uses a vector $\boldsymbol{\varphi_{vec}}$ with $|\varphi_{vec}(i+1) - \varphi_{vec}(i)| = \delta$, $i = \{1,2,\dots,N_{vec}\}$ steering points corresponding to the centre of the small windows. The NT SLM is continuously scanning through this vector until light is detected by the Quad ($OP_Q > TH_{OP}$, here TH_{OP} is a predefined optical power threshold). The tracking state ($ST = 2$) is then turned on. The beam is iteratively steered to the centre depending on the sign of the Quad differential reading $\Delta H = P_A + P_C - P_B - P_D$. Once $|\Delta H|$ is below a predefined threshold TH_{POS}, then the beam is considered aligned. The system passes to an idle state ($ST = 3$) until either the beam drifts away from the Quad centre ($|\Delta H| > TH_{POS}$) or altogether out of the Quad active area ($OP_Q > TH_{OP}$).

The iteration in the tracking state ($ST = 2$) is required

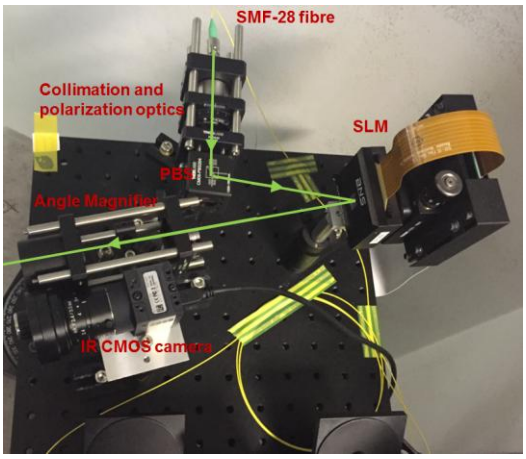

Figure 7. Base station experimental layout including the IR localization CMOS camera. PBS is a polarization beamsplitter.

because the Quad gives limited information about the beam position. That is, although these type of devices are high precision position sensors [16], they also require smooth transverse intensity profiles to estimate the beam position [17]. In our setup, the beam is far from a perfect Gaussian or other known deterministic profile due to geometrical aberrations and aperture vignetting distortions at the NT. Therefore, the differential Quad signal ΔH is only used to know whether the beam is to the left or right of the Quad centre. Other PSD devices such as lateral effect sensors or InGaAs 1550 nm cameras could give a direct reading of the beam position with higher degree of independence on the beam profile. These devices are good candidates for future implementations requiring a faster tracking response.

Finally, the search and track algorithm can be extended to a direction normal to the horizontal axis. This is straightforward by using φ_V as the vertical steering variable and the Quad vertical reading $\Delta V = P_A + P_B - P_C - P_D$. However, the vector $\boldsymbol{\varphi_{vec}}$ becomes a matrix with N_{vec}^2 elements, which in turn slows down the search algorithm. In the experiments, the NT was considered moving mainly in the horizontal direction. Thus, the search algorithm was kept in 1D. The tracking states though were implemented for both the horizontal and vertical directions.

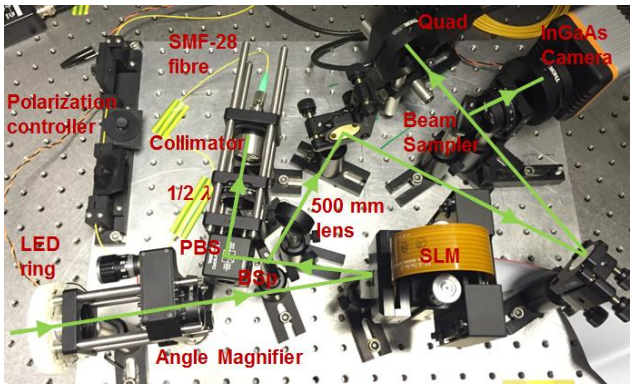

Figure 8. NT experimental layout with the added Quad tracking components. BSp is a beamsplitter and PBS is a polarization BSp. InGaAS camera for characterising the signal beam distribution

C. *Preliminary experiments*

Preliminary experiments were carried out to test the BS localization and NT tracking modules individually.

1) *BS localization*

The CMOS camera performance was initially tested. The LED ring was located at a distance of 3 m. The image was captured every second for 100 seconds, and the LED ring centre was estimated for all N = 100 images. The largest deviation between any two centres in the sample was found to be 0.2 pixels. This corresponds to an angular error of 0.05º or 2.5 mm for d_{NT} = 3 m. Therefore the proposed camera based localization system is sufficiently accurate.

The required BS calibration described in section II.A.3) was also carried out for the experimental setup shown in Figure 7. The CMOS camera was placed next to an AM-SLM-based beamsteering module with a FOV = $\pm 30°$. The SLM not only performed the basic steering function but also corrected for geometrical aberrations introduced by the AM [10]. It was deduced that N_{scan} = 12 (see section II.A.3) was sufficient for a 1D horizontal steering calibration. This is equivalent to having a calibration point every 5°. A 2D calibration was not needed in this simplified case as the experiments were kept in a plane parallel to the optical table.

2) *NT tracking*

The NT tracker requires a steering accuracy of $\Delta\delta = 0.1°$ as shown in Figure 2 (b). This keeps the fibre coupling loss below 3 dB for an SMF-based receiver. For the Quad-lens design a lens (Thorlabs AC254) with f_Q = 500 mm and clear aperture $a_L \sim$ 11.5 mm was chosen. At the same time, a Quad (Thorlabs PDQ30C) with a_Q = 1.5 mm was used. Considering a beamsteering SLM (BNS HSP512-1550) with an active area $\omega_{SLM} \sim 3.5\,mm$ and a steering range $\delta = \pm 3°$, $\Delta S_Q(\delta = \pm 3°) = \pm$ 26.2 mm was obtained by fixing $d_Q \sim f_Q$. This corresponds to a full displacement window of 52.4 mm in the Quad plane, which is ~ 17 times larger than the Quad active area diameter $2a_Q$ = 3 mm. Therefore, a software-based (MATLAB) search and tracking system was implemented based on Figure 6 flowchart with N_{vec} = 17.

An SLM to lens distance $d_{SLM} \sim$ 100 mm was also set to avoid any vignetting of the incident beam beyond the lens aperture. The final NT setup including the Quad is shown in Figure 8. The next section describes the joint performance of the BS and NT in a functional ultra-high data rate link.

III. TRANSMISSION EXPERIMENT

A test-bed was designed to characterize the IR localization at the BS as well as the NT Quad-based alignment as function of the link angle θ_l. Figure 9 shows the corresponding schematic at a transceiver's range of Z = 2.8 m. This distance was kept constant throughout the experiments. The BS is mounted on a rotation stage driven by a Newport ESP300 driver with 0.0002º accuracy. The rotation axis is located at the AM exit aperture defining the BS link angle θ_l^{BS}. On the receiver side of the link, the NT is mounted on a breadboard that can be manually rotated around its AM entrance aperture

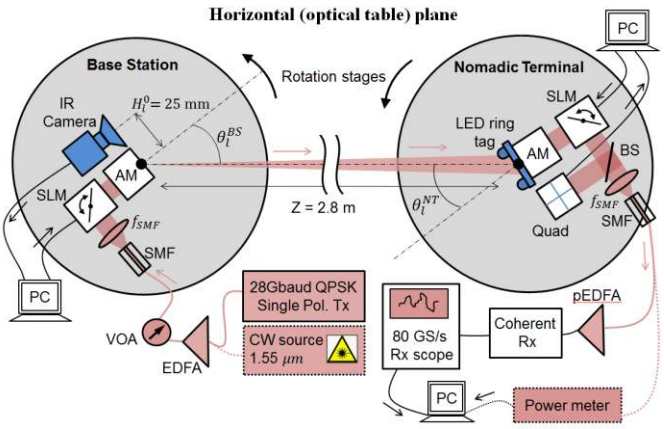

Figure 9. Communications test-bed. The base station and the nomadic terminal are mounted on rotation stages. BS is a beamsplitter with 90% transmission / 10 % reflection coefficients. Also, f_{SLM}= 37 mm is the focal length of a SMF pigtailed focusing lens with NA = 0.24. VOA is a variable optical attenuator. Also, pEDFA is a preamplifier EDFA.

as well. This determines the NT link angle θ_l^{NT}.

The CMOS camera localization at the BS and the NT Quad-based search and tracking were implemented in Matlab® using different PCs for each transceiver. The aligned link performance was characterized using either a CW 1550 nm laser, or a standard coherent transmission system. For the latter implementation, the achieved data rate was 50 Gb/s. In the following sections these experiments are discussed in detail.

A. *CW study*

A 1550 nm CW laser was connected to the BS SMF input as shown in Figure 9. The BS station was rotated to an arbitrary angle θ_l^{BS}. The NT was also rotated to an approximately equal angle $\theta_l^{NT} \sim \theta_l^{BS}$. Provided a proper calibration of the IR localization and NT Quad-based alignment systems, an automated link alignment can be successfully established after several seconds. Thus, the system is considered nomadic rather than mobile (the use of faster components in future implementations could make the system respond in real-time).

The localization and tracking process consists of two states. First, a transient state defined by the time it takes the BS and the NT to properly align with respect to each other. And second, a stable state where the link remains aligned subject to minor perturbations due to mechanical vibrations, small NT movements within the communications beam footprint, or other sources of errors.

For a stable state, Figure 10 shows a comparison between the manually optimized alignment and the automated cases. The BS localization system adds a penalty of maximum 3 dB for the scanned FOV of 30º. Small additional drops are seen in the received power when including the NT Quad-based tracking. Improvements in the Quad mechanical pre-alignment can reduce this effect.

NT displacements beyond ~ 10 mm can take the system back to the transient state. The corresponding recovery response is variable and depends on the NT motion speed and

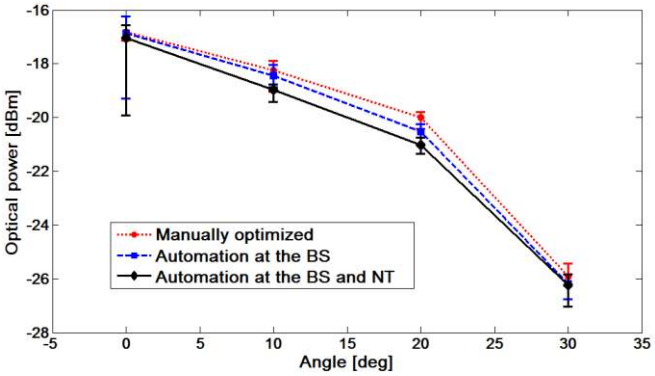

Figure 10. Coupled optical power at the NT as a function of the link angle θ_l. The alignment was either manually optimized, automated for the BS localization system or automated for both the BS localization and NT tracking systems.

new position. The blockage of the BS-NT line-of-sight (LOS) also brings the system into the transient state but the process is more predictable. If the LOS between the BS and NT is lost, then the BS memorizes its previous position until the beacon reappears. However, the NT goes to a beam search state ($ST = 2$ in Figure 6) scanning through the whole FOV to steer the beam back to the Quad active area. The recovery time of the system after momentarily blocking the communications beam is on the order of seconds.

Finally, the tracking response in the stable state was studied. For this purpose, the BT was rotated in steps of 0.1º around $\theta_l = 30°$. This corresponds to a NT displacement of ~ 5 mm at a BS-NT distance of Z = 2.8 m, hence the beam is misaligned but still illuminates the NT aperture. The results are given in Figure 11. It can be seen that the BS localization and NT tracking recover the link in less than 5 seconds. With no automated localization and tracking system, there is a permanent drop (as much as 3 dB) in the received power.

B. *Communications link*

In this section the performance of a coherent transmission link subject to the effects of the automated alignment is given. For this purpose, a 28Gbaud single polarization quadrature phase shift keying (QPSK) transmitter [18] is connected to the BS via an EDFA as shown in Figure 9. Also, the NT SMF is connected to an intradyne coherent receiver via a removable

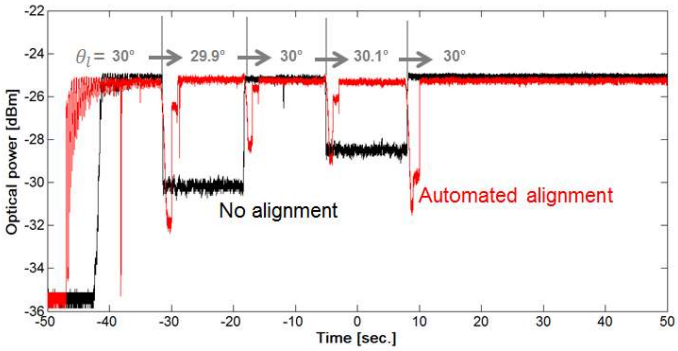

Figure 11. Received optical power at the NT as a function of time. The red curve corresponds to an automated tracking for the BS and NT. The black curve is for a system with no tracking.

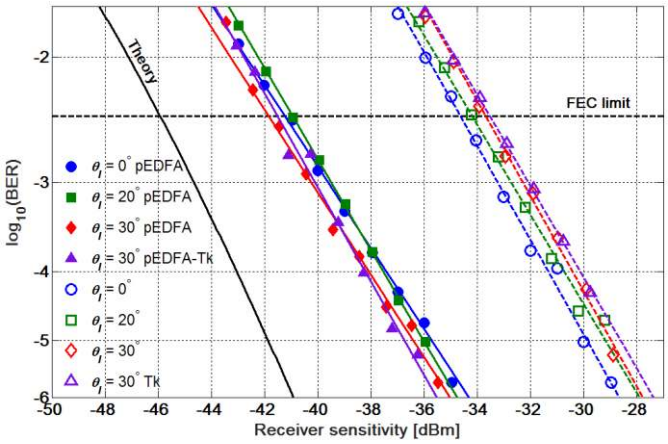

Figure 12. Coherent receiver sensitivity. The filled markers with solid lines represent the results with optical pre-amplification (pEDFA) while the open markers with dotted lines represent the results without pre-amplification. Tk means the BS tracking is ON.

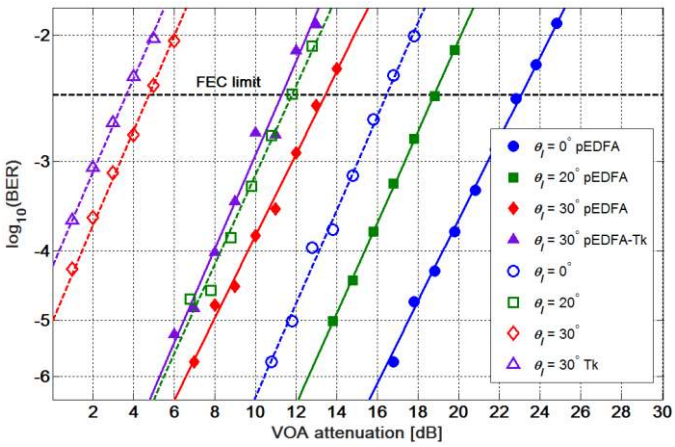

Figure 14. BER vs VOA attenuation. The filled markers with solid lines represent the results with optical pre-amplification (pEDFA) while the open markers with dotted lines represent the results without pre-amplification. Tk means the BS tracking is ON.

preamplifier EDFA. The receiver output signal is finally captured by a real-time oscilloscope sampling at 80 GS/s. The transmission tests last for ~ 38 μs which corresponds to the size of the oscilloscope sampling window. Further off-line processing takes ~ 1 min. Therefore, the transient state of the automated alignment process could not be monitored. We focused on the link's stable state once the BS and NT are aligned.

Figure 12 shows the sensitivity curves for different link angles θ_l and the optional use of the BS tracking and / or EDFA pre-amplifier. It can be seen that the sensitivity is independent of the NT tracking and link angles with a ~1 dB penalty at the forward error correction (FEC) limit, with and without optical pre-amplification. However, the removal of the EDFA preamplifier produces an average of ~7 dB drop in the link margin.

To characterize the BS localization system, a statistical approach was used, in which 100 communications captures were run with a 1 minute difference between consecutive capture, which is sufficient for the delay of the offline DSP. The variable optical attenuator (VOA) was set such that system performance was near the FEC limit of the coherent receiver. Results are given in Figure 13. The histograms show a less than 1 dB broadening in the sample distribution due to the BS localization error characterized in section II.C.1). The

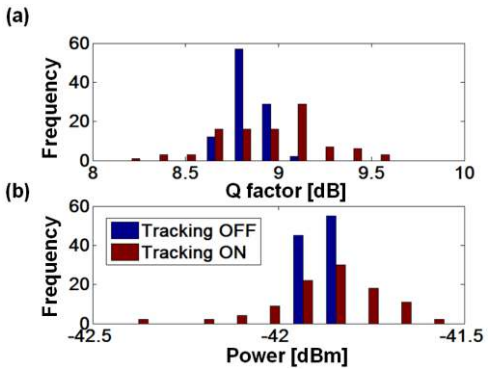

Figure 13. Histograms of optical power and Q-factor for the coherent receiver with EDFA pre-amplification. The sample size is 100.

shifts in the histograms' peaks indicate that the link with automated tracking was better aligned.

Finally, the link BER performance as a function of the VOA attenuation was measured, whilst keeping the BS optical output power at 10 dBm (eye-safe 1550 nm limit). Figure 14 shows the results for different configurations depending on the use of BS tracking, EDFA pre-amplification and link angle. For each configuration, the interception of the curve with the FEC limit gives the available power budget, i.e. the maximum allowed optical loss in an error-free communications link.

The power budget is strongly reduced as θ_l increases. From $\theta_l = 0°$ to 20° the drop is ~ 4 dB for both configurations (with and without EDFA preamplifier). However, when changing from $\theta_l = 20°$ to 30° the power budget reduces by as much as 7 dB. This is because, for large θ_l, the link suffers much higher geometrical aberrations, vignetting and steering losses which reduces the optical coupling into the receiver SMF fibre. It can also be seen that the automated BS localization at $\theta_l = 30°$ produces a power budget reduction of up to ~ 2 dB, considering both the link with EDFA preamplifier and without it. For a different θ_l, the penalty depends on the corresponding pre-calibration, although it will be less critical as the power margin increases.

IV. Conclusions

A localization and tracking system has been successfully designed and implemented, suitable for ultrafast narrow beam indoor optical wireless communications requiring alignment at both ends of the link. A localization accuracy of 0.05° was achieved for an SMF-wireless-SMF geometry. Using this system, a 50 Gb/s QPSK coherent transmission with automated alignment for the whole FOV of ±30° at a range of up to 3 m was demonstrated. The localization and tracking systems added penalties of up to 2 dB compared to the manually aligned cases. Also, the use of an EDFA preamplifier at the receiver improved the link margin by as much as 7 dB.

This demonstration paves the way for narrow beam indoor

mobile wireless communications with the potential of data rates beyond 100 Gb/s. The link is inherently bidirectional and the use of SLMs makes point-to-multipoint architectures feasible. Future work should focus on faster implementations of the CMOS camera and image processing for the BS localization system. The NT tracking module may be enhanced by the use of position sensing detectors with relative independence of the beam intensity profile.

ACKNOWLEDGMENT

The research is funded by the UK Engineering and Physical Sciences Research Council (EPSRC) under grants EP/J008842/1 (COMIMO project) and 1181352 (Future Optical Wireless Communications).

REFERENCES

[1] "The Zettabyte Era : Trends and Analysis," 2015.

[2] M. Weiss, a. Stohr, F. Lecoche, and B. Charbonnier, "27 Gbit/s photonic wireless 60 GHz transmission system using 16-QAM OFDM," *2009 Int. Top. Meet. Microw. Photonics*, pp. 9–11, 2009.

[3] T. S. Rappaport, R. Mayzus, Y. Azar, K. Wang, G. N. Wong, J. K. Schulz, M. Samimi, and F. Gutierrez, "Millimeter Wave Mobile Communications for 5G Cellular: It Will Work!," *IEEE Access*, vol. 1, pp. 335–349, 2013.

[4] S. Rangan, T. S. Rappaport, and E. Erkip, "Millimeter-wave cellular wireless networks: Potentials and challenges," *Proc. IEEE*, vol. 102, no. 3, pp. 366–385, 2014.

[5] S. Koenig, D. Lopez-Diaz, J. Antes, F. Boes, R. Henneberger, a. Leuther, a. Tessmann, R. Schmogrow, D. Hillerkuss, R. Palmer, T. Zwick, C. Koos, W. Freude, O. Ambacher, J. Leuthold, and I. Kallfass, "Wireless sub-THz communication system with high data rate," *Nat. Photonics*, vol. 7, no. 12, pp. 977–981, 2013.

[6] T. Kleine-Ostmann and T. Nagatsuma, "A review on terahertz communications research," *J. Infrared, Millimeter, Terahertz Waves*, vol. 32, no. 2, pp. 143–171, 2011.

[7] D. Tsonev, H. Chun, S. Rajbhandari, J. J. D. Mckendry, S. Videv, E. Gu, M. Haji, S. Watson, A. E. Kelly, G. Faulkner, M. D. Dawson, H. Haas, and D. O. Brien, "A 3-Gb / s Single-LED OFDM-Based Wireless VLC Link Using a Gallium Nitride μ LED," *Photonics Technol. Lett.*, vol. 26, no. 7, pp. 637–640, 2014.

[8] K. Wang, S. Member, A. Nirmalathas, S. Member, C. Lim, and E. Skafidas, "4 x 12 . 5 Gb / s WDM Optical Wireless Communication System for Indoor Applications," *J. Light. Technol.*, vol. 29, no. 13, pp. 1988–1996, 2011.

[9] M. Maier, M. Lévesque, and L. Ivanescu, "NG-PONs 1&2 and Beyond: The Dawn of the Uber-FiWi Network," *IEEE Netw.*, no. March, pp. 15–21, 2012.

[10] A. Gomez, K. Shi, C. Quintana, M. Sato, G. Faulkner, B. C. Thomsen, and D. O. Brien, "Beyond 100-Gb / s Indoor Wide Field-of-View Optical Wireless Communications," *Photonics Technol. Lett.*, vol. 27, no. 4, pp. 367–370, 2015.

[11] K. Wang, A. Nirmalathas, C. Lim, and E. Skafidas, "High-speed indoor optical wireless communication system with single channel imaging receiver," *Opt. Express*, vol. 20, no. 23, p. 25356, Nov. 2012.

[12] C. W. Oh, E. Tangdiongga, and a. M. J. Koonen, "Steerable pencil beams for multi-Gbps indoor optical wireless communication," *Opt. Lett.*, vol. 39, no. 18, p. 5427, Sep. 2014.

[13] K. Wang, A. Nirmalathas, C. Lim, and E. Skafidas, "Experimental Demonstration of a Centralized Optical Wireless Indoor Localization System for High-Speed Communications in Personal Areas," vol. 40, no. 7, pp. 3–4, 2013.

[14] Y. Gu, A. Lo, and I. Niemegeers, "A survey of indoor positioning systems for wireless personal networks," *IEEE Commun. Surv. Tutorials*, vol. 11, no. 1, pp. 13–32, 2009.

[15] A. Gomez, C. Quintana, G. Faulkner, and D. O. Brien, "Challenges in Wide Coverage Indoor Optical Communications Using Fibre-Wireless-Fibre Links for Terabit data rates," in *IEEE GlobeCom*, 2015.

[16] K.-C. Fan, C.-L. Chu, J.-L. Liao, and J.-I. Mou, "Development of a high-precision straightness measuring system with DVD pick-up head," *Meas. Sci. Technol.*, vol. 14, no. 1, pp. 47–54, 2002.

[17] Y. Panduputra, T. W. Ng, A. Neild, and M. Robinson, "Intensity influence on Gaussian beam laser based measurements using quadrant photodiodes.," *Appl. Opt.*, vol. 49, no. 19, pp. 3669–3675, 2010.

[18] K. Shi, A. Gomez, X. Jin, Y. Jung, C. Quintana, D. O. Brien, F. P. Payne, P. Barua, J. Sahu, Q. Kang, S. Alam, and D. J. Richardson, "Simplified Impulse Response Characterization for Mode Division Multiplexed Systems," in *Optical Fiber Communication Conference*, 2016, p. paper W4F.3.